ANALYTICAL SCIENCES DECEMBER 2020, VOL. 36

A Pterin-FAM-TAMRA Tri-color Fluorescence Biosensor to Detect the Level of KRAS Point Mutation

Ni ZENG, Yaxin GUO, and Juan XIANG†

College of Chemistry and Chemical Engineering, Central South University, Changsha 410083, PR China

Monitoring the changes in the level of KRAS point mutation (the concentration fraction of the KRAS point mutated DNA to the total DNA) in clinical treatment progress can guide and greatly improve the personalized therapy and therapeutic evaluation of patients with cancer. In this work, based on FRET fluorescence quenching and apyrimidinic site-induced guanine/pterin specific binding, we developed a pterin-FAM-TAMRA tri-color fluorescence sensing system to assess the level of KRAS point mutation in one step. The responses from TAMRA displayed good and similar linear correlations in the range from 60 nM to 2 μM for all four types of DNA, resulting in a common linear equation related to the T-DNA concentration ($N_{\Delta FTAMRA} = 2.908c_{T\text{-}DNA} + 0.364$). Meanwhile, the responses from pterin showed excellent selectivity to W-DNA and an excellent linear correlation to the W-DNA in the concentration range from 60 nM to 1 μM ($N_{\Delta Fpterin} = -0.364c_{gDNA\text{-}G} + 0.034$). This biosensor has an effective concentration range for detecting KRAS point mutations. Especially, because the apyrimidinic site-induced guanine/pterin binding is selective for the detection of wild-type DNA, the sensing system can be applied for clinical mutation level detection of all kinds of KRAS point mutations (G → A, G → C and G → T) in blood samples, which is crucial for the personalized therapy and therapeutic evaluation of patients with most KRAS-related cancer types.

Keywords KRAS, mutation level, tri-color fluorescence sensor, apyrimidinic site

(Received July 20, 2020; Accepted August 13, 2020; Advance Publication Released Online by J-STAGE August 21, 2020)

Introduction

Kirsten rat sarcoma viral gene (KRAS) instructs the synthesis of a 21 kDa Ras protein, which is a portion of the signal pathway of the RAS/MAPK.[1] When mutated, the KRAS gene has the potential to cause uncontrollable and cancerous cell proliferation. Almost 25% of all kinds of cancers contain KRAS mutations.[2] Particularly, KRAS mutations appear in 90% of pancreas cancers,[3,4] ~40% of metastatic cancers[5] and 33% of non-small cell lung cancers.[6,7] Therefore, KRAS point mutations have been identified as one of the crucial biomarkers for tumor-targeting diagnosis and therapy. In recent years, in order to detect KRAS point mutations, numerous methods have been developed, including Sanger sequencing,[8] pyrosequencing,[9] digital polymerase chain reaction,[10] and next-generation sequencing.[11] These methods can fulfill the quantification of DNA and identification of the genotype. However, the majority of these systems are time-consuming and costly with the requirement for a larger volume of samples. In order to accomplish more rapid and low-cost detection, a variety of different studies were developed, including multi-target digital droplet PCR,[12] nest hybridization chain reaction,[13] AuNP-based colorimetric assay,[14] peptide nucleic acid-PCR,[15] MASA-PCR,[16,17] denaturing high performance liquid chromatography system[18] and anchor-like DNA electrochemical biosensor.[19] Although the majority of the above-mentioned systems enable time-saving and low-cost detection of KRAS point mutations, these systems have shortcomings in clinic applications.

KRAS point mutation occurs in codons 12, 13 or 61.[20,21] The most common mutation occurs in codon G12, including G12D, G12A, G12C, G12V, G12R and G12S.[22-25] Methods in G12D (GGT → GAT) and G12V (GGT → GTT) account for 58% of all KRAS mutations in cancers.[26] Recently, there have been significant advancements in the identification of genetic alteration sensitivity to cancer therapeutics. As clinical treatment progresses, the contents of both wild and mutated DNA change significantly. Monitoring these changes can guide and greatly improve the personalized approach to patient treatment and therapeutic efficacy evaluation. Meanwhile, compared with the concentration of KRAS point mutation, the level of KRAS point mutation, which is defined as the proportion of concentration of the mutant DNA to the total DNA (T-DNA, including KRAS mutant DNA and wild-type DNA), has been identified as a more effective index. Due to the diverse types of KRAS mutations, expensive multichannel techniques were usually employed in the clinic to follow the mutation level changes.[27] Although some simple methods such as anchor-like DNA biosensors and droplet digital PCR have been developed, they can only detect one type of KRAS point mutation. Development of strategy allowing for general, cost-effective and rapid KRAS mutation level detection is still needed.

Herein, we constructed a pterin-FAM-TAMRA tri-color fluorescence sensing system based on FRET fluorescence quenching and apyrimidinic site-induced guanine/pterin specific binding to deal with these challenges. By simultaneously

N. Z. and Y. G. contributed equally to this work.
† To whom correspondence should be addressed.
E-mail: xiangj@csu.edu.cn

detecting the wild-type and the total DNA, the mutation level can be easily achieved in one step. This tri-color fluorescence sensor is low-cost, selective and easy to assemble and operate. Meanwhile, this biosensor has an effective concentration range for detecting KRAS point mutations. Especially, because our detection is selective to the wild-type DNA, the sensing system can be applied for monitoring the mutation level in all kinds of KRAS mutations, including G12D, G12S (G → A), G12A (G → C) and G12V, G12C (G → T). It means it is crucial for personalized therapy and therapeutic evaluation of patients with most types of KRAS-related cancers.

Experimental

Reagents

All oligonucleotides were HPLC-purified and purchased from Shanghai Sangon Biotechnology Co., Ltd. (Shanghai, China) and the sequences of all oligonucleotides are listed in Table 1. 2-Amino-4-hydroxypteridine ($C_6H_7N_5O$, pterin), tris-(hydroxymethyl)aminomethane (tris), ethylenediaminetetraacetic acid (EDTA), HCl, Na_2HPO_4, NaH_2PO_4, NaCl, KCl, $MgCl_2$ and $CaCl_2$ were purchased from Aladdin Industrial Co., Ltd. (Shanghai, China). Milli-Q water (18.2 MΩ cm, Millipore M-Q system Inc., Milford, MA, USA) was used in all experiments.

Instrumentation

All measurements of fluorescence were carried out on the FL-4600 fluorescence spectrometer (Hitachi, Japan). The excitation slits and emission slits were 10.0 nm. Also, the voltage of the photomultiplier tube was 700 V. The scanning wavelength in the pterin-FAM-TAMRA sensing system was collected from 380 to 700 nm with an excitation wavelength at 360 nm. All fluorescence measurements were performed at room temperature (25°C).

Preparation for fluorescence detection

All oligonucleotide (MB-DNA, gDNA-G, gDNA-A, gDNA-C and gDNA-T) stock solutions were prepared with 34 mM Tris–HCl buffer (pH 7.4).[28] The MB-DNA solutions were put at 85°C for 5 min. Then the solutions cooled down to room temperature to form a hairpin-structured molecular beacon DNA probe (pMB-DNA). After that, pterin was added in the dark to construct the tri-color fluorescence system with the final pterin and pMB-DNA concentration of 0.5 and 2 μM, respectively. Before fluorescence spectra measurement, gDNA was added into the tri-color fluorescence system and incubated at 37°C for 2 h.

Preparation of human serum samples

The samples of healthy human blood were provided by Xiangya Hospital Central South University (Changsha, China). All the agreements were examined by The Joint Ethics Committee of the Central South University Health Authority and then performed in accordance with national guidelines. All samples were centrifuged at 2000 rpm for 15 min. Then 100 kDa ultra-filtration membranes were used to reduce the interference of co-existing proteins. After that, the obtained samples of normal human blood were deposited at –20°C for later use. Finally, the solution was diluted 10 times with phosphate buffered saline (PBS, pH 7.4) before each test.

Table 1 Names and sequences of the oligonucleotides in this work

Names	Sequence (5′ → 3′)
MB-DNA	FAM-TTAATTTACGCCA/dSpacer/CAGCTCCAATTAA-TAMRA
gDNA-G	GGAGCTG**G**TGGCGTA
gDNA-A	GGAGCTG**A**TGGCGTA
gDNA-C	GGAGCTG**C**TGGCGTA
gDNA-T	GGAGCTG**T**TGGCGTA

The underlined sequences of MB-DNA represent the matching segments in the molecular beacon DNA (MB-DNA). The underlined bold bases display the difference in four target gDNAs. Here, gDNA-G corresponds to the wild-type DNA while the other three types are mutations.

Results and Discussion

Sensing principle

In this work, a pterin-FAM-TAMRA tri-color fluorescence sensing system was constructed to detect the amount of T-DNA and W-DNA in the KRAS mutation in one step. As shown in Fig. 1, the pterin-FAM-TAMRA tri-color sensing system includes the mixture of hairpin-structure probe DNA (pMB-DNA) and pterin. The pMB-DNA, prepared from the self-hybridization of molecular-beacon DNA (MB-DNA), is labeled with FAM and TAMRA fluorescent molecules at both ends of the DNA strand. In the loop, an apyrimidinic (AP) site is designed to be located opposite the variable base site in the gDNAs. The entire detection process can be described as below. In the absence of gDNA, FAM is close to TAMRA in the hairpin

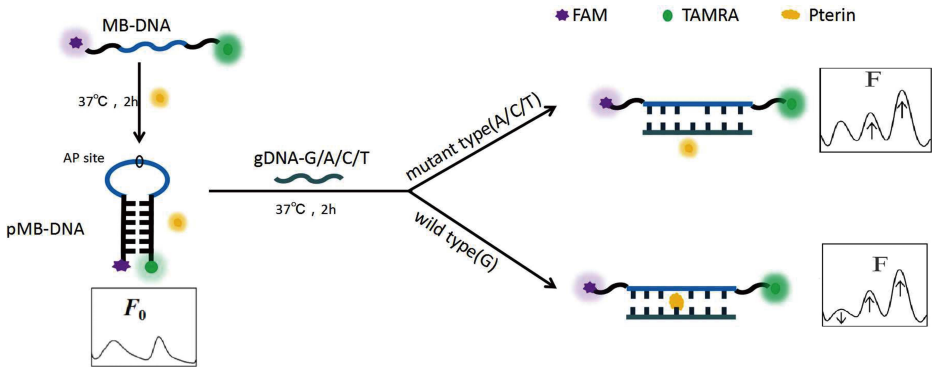

Fig. 1 Schematic representation of the detection of the level of KRAS point mutation with the proposed pterin-FAM-TAMRA tri-color sensing system.

structure. Since the emission spectrum of FAM overlaps with the absorption spectrum of TAMRA, fluorescence resonance energy transfer (FRET) occurs,[29] which has been used in many works related to DNA detection.[30,31] The fluorescence of FAM is absorbed by TAMRA and appears as a fluorescence quenching state, while the signal from TAMRA is also attenuated due to the interaction. Then, the disappearance of FAM emission at 520 nm can be used to evaluate the formation of hairpin-structured pMB-DNA. With the addition of pterin to the pMB-DNA solution, the mixed sensing system will give a strong pterin emission peak at 440 nm with a weak TAMRA peak centered at 582 nm. Once the gDNA is added, the hairpin structure will be broken to form a rigid duplex structure because the T-DNA is hybridized with the loop of pMB-DNA. As a result, the fluorescence intensity of FAM and TAMRA will increase proportionally to the T-DNA concentration. Meanwhile, pterin, acting as a hydrogen-bonding ligand, can selectively recognize G base opposed to the AP site.[32,33] It means that only the wild-type gDNA-G can be indicated by pterin. In this case, pterin enters the hydrophobic cavity provided by the AP site in the double-stranded oligonucleotides and binds to guanine *via* a three-point hydrogen-bonding. Guanine, a compound with multiple electron-giving groups, is liable to lose electrons, which can be transferred to the electron orbital of pterin, leading to fluorescence quenching.[34] Therefore, according to the simultaneous fluorescence quenching of pterin and enhancing of FAM/TAMRA, the W-DNA and T-DNA can be quantified, respectively. Then, the mutation level can be achieved as $1\text{-}c_{\text{W-DNA}}/c_{\text{T-DNA}}$.

Compared with traditional fluorescent biosensors based on the molecular beacon and FRET principle, our tri-color sensing system has the following advantages. First, the sensor realizes the detections of both W-DNA and T-DNAs in one step. It is low-cost, time-saving, and more practical than the traditional single output sensor. Second, the initial sensor structure can be evaluated by the disappearance of the FAM signal, which improves the reproducibility of the detection. Third, this sensor evaluates the mutation level *via* quantifying the wild-type DNA, which is available for monitoring all kinds of KRAS mutations in codon G12 (G → A, G → C, and G → T). This general method for mutation level detection can be widely applied for personalized treatment and therapeutic efficacy evaluation for most KRAS-related cancer patients.

Feasibility of the tri-color sensing system

To verify the feasibility of the designed tri-color sensing system, the typical fluorescence responses of the sensor in the presence of four gDNAs were performed. As shown in Fig. 2, in the absence of gDNA, the fluorescence spectra displayed obvious pterin (~440 nm) and TAMRA signals (~582 nm). The disappearance of FAM emission at 520 nm confirms the formation of the hairpin structure in the pMB-DNA. With the addition of gDNA, the FAM emission appears at ~520 nm, which is attributed to the formation of DNA duplexes, breaking the hairpin structure of the pMB-DNA. Also, the emission of TAMRA at ~582 nm is significantly enhanced. Compared with FAM, TAMRA displays much more significant enhancement. Therefore, in our strategy, the enhanced fluorescence intensity from TAMRA, ΔF_{TAMRA}, was used to quantify the T-DNA.

Although four gDNAs induced similar changes on FAM and TAMRA signals, their effects on pterin are quite different. The wild-type gDNA-G significantly reduces the fluorescence intensity of pterin, while the other three mutations (gDNA-A, gDNA-A, and gDNA-T) induce no detectable changes on pterin's emission. The specific recognition is ascribed to the entry of pterin into the hydrophobic cavity provided by the AP site in the double-stranded DNA and subsequent formation of non-fluorescent intermediate complex guanine/pterin. It confirms the feasibility of pterin signal changes ΔF_{pterin} for the quantitation of W-DNA.

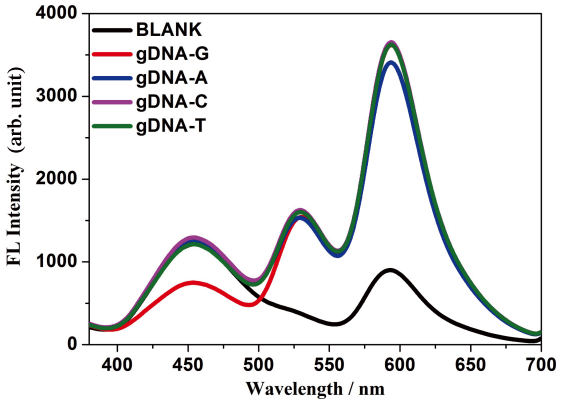

Fig. 2 Fluorescence spectra of the tri-color fluorescent sensor with the presence of different gDNAs. The concentration of pterin and MB-DNA is 0.5 and 2 μM, respectively. All the gDNA solutions are 2 μM.

Optimization of experimental conditions

According to our detection strategy, the enhanced TAMRA fluorescence intensity ΔF_{TAMRA} is used to quantify the T-DNA. To achieve good sensor performance, all four gDNAs are expected to induce sensitive responses to ΔF_{TAMRA}. Meanwhile, the quenched pterin fluorescence intensity ΔF_{pterin} is used to selectively quantify the W-DNA. Only the wild-type gDNA-G is anticipated to respond to ΔF_{pterin}. Based on this, we systematically studied the effects of buffer solution, pH value and hybridization time on the gDNA-induced fluorescence changes ΔF_{pterin} and ΔF_{TAMRA} to reveal the optimal experimental conditions. As shown in Fig. 3A, among three typical buffers (PB, PBS and Tris–HCl), PBS provides the largest ΔF_{TAMRA} value with the smallest relative standard deviation for all four gDNAs. Meanwhile, gDNA-G induces a large ΔF_{pterin} value without obvious disturbance from the other three gDNAs. It indicates that PBS is a better choice over PB and Tris–HCl for our sensor system. Based on this, the pH effect of PBS buffer on the detection was further investigated. Since basic conditions disfavor the DNA hybridization,[35] we studied the effect under weak acidic and neutral conditions. As shown in Fig. 3B, with the increase of the solution pH from 6.8 to 7.4, both ΔF_{pterin} and ΔF_{TAMRA} are enhanced significantly. Therefore, pH 7.4 was used as the optimal pH. The effect of DNA hybridization time was also studied. As shown in Fig. 3C, with the increase of the hybridization time from 30 to 120 min, the ΔF_{TAMRA} values from four gDNAs are in a close range. Meanwhile, the ΔF_{pterin} from gDNA-G increases gradually, but the responses from the other three gDNAs are not obvious. It indicates the long hybridization time is better. Therefore, PBS buffer at pH 7.4 and hybridization time of 120 min were confirmed as the optimal conditions for the sensor system. One thing that should be mentioned is under these optimal conditions, both ΔF_{pterin} and ΔF_{TAMRA} display small and close relative standard deviations for all four gDNAs. It ensures the good reproducibility of the detection.

Quantification detection of T-DNA and W-DNA

Four gDNAs with different concentrations were detected with our tri-color fluorescence biosensor. In order to reduce the

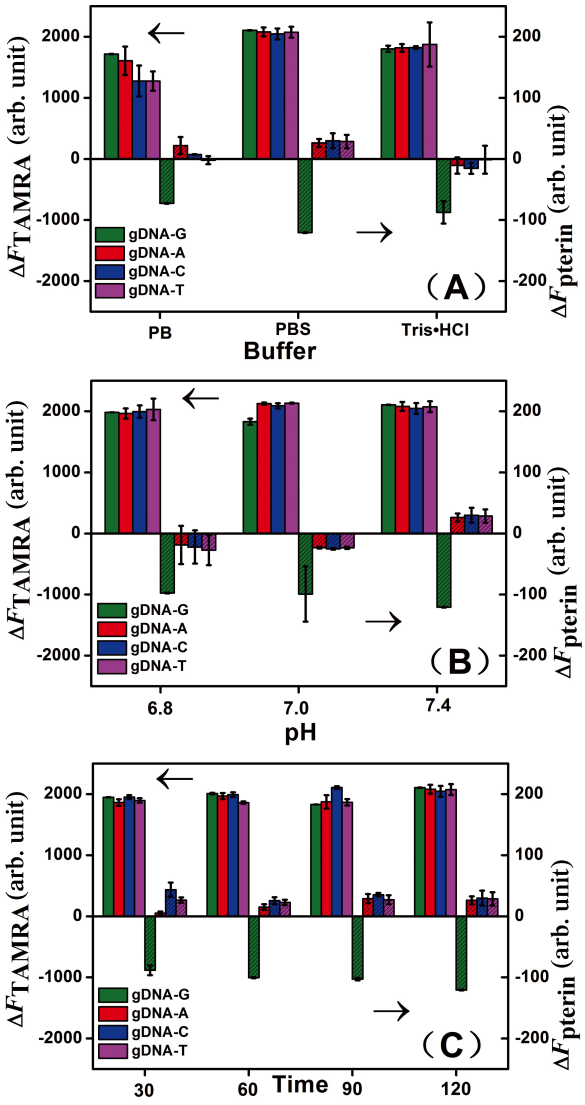

Fig. 3 Effects of buffer solution's composition (A), pH value (B) and hybridization time (C) on gDNA-induced fluorescence changes ΔF_{TAMRA} (solid columns) and ΔF_{pterin} (sparse filled columns). The corresponding error bars represent the standard deviation of three parallel experiments.

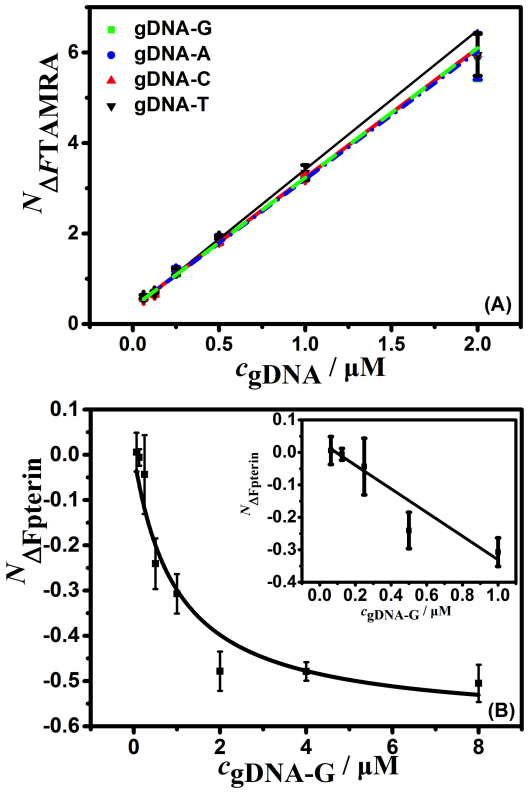

Fig. 4 Detections of the T-DNA and W-DNA. (A) The linear relationships between $N_{\Delta FTAMRA}$ and the corresponding concentrations of four different gDNAs. (B) The relationship between $N_{\Delta Fpterin}$ and c_{gDNA-G}. Error bars represent the standard deviation of three independent determinations. Inserted is the linear calibration curve between $N_{\Delta Fpterin}$ and c_{gDNA-G}.

Table 2 Recovery rates of the T-DNA in 10-fold-diluted blood serum samples from healthy persons

T-DNA	Added/μM	Found/μM	Recovery, %	RSD, %
1	0	0	—	—
2	0.1	0.0975 ± 0.003	97.5	3.15
3	1.0	0.9748 ± 0.006	97.5	0.62
4	2.0	1.9202 ± 0.159	96.0	8.27

Table 3 Recovery rates of the W-DNA in 10-fold-diluted blood serum samples from healthy persons

W-DNA	Added/μM	Found/μM	Recovery, %	RSD, %
1	0	0	—	—
2	0.1	0.096 ± 0.004	96.0	4.20
3	0.5	0.527 ± 0.014	105.4	2.62
4	1.0	1.039 ± 0.048	103.9	4.67

systematic error, both fluorescence intensity changes (ΔF_{pterin} and ΔF_{TAMRA}) were compared with the corresponding initial intensity in the blank solution and expressed as $N_{\Delta\text{Fpterin}}$ and $N_{\Delta\text{FTAMRA}}$, respectively. Figure 4A displays the dependence of $N_{\Delta\text{FTAMRA}}$ on the concentrations of four different gDNAs. As expected, all four gDNAs display similar and good linear responses with the dynamic range from 60 nM to 2 μM (280 – 9378 ng/mL). The obtained linear equations are very close ($N_{\Delta\text{FTAMRA}} = 2.868c_{\text{gDNA-G}} + 0.367$ ($R = 0.9996$), $N_{\Delta\text{FTAMRA}} = 2.828c_{\text{gDNA-A}} + 0.372$ ($R = 0.9992$), $N_{\Delta\text{FTAMRA}} = 2.861c_{\text{gDNA-C}} + 0.373$ ($R = 0.9991$), $N_{\Delta\text{FTAMRA}} = 3.074c_{\text{gDNA-T}} + 0.344$ ($R = 0.9921$)). On the basis of this, a common linear equation for T-DNA concentration, $N_{\Delta\text{FTAMRA}} = 2.908c_{\text{T-DNA}} + 0.364$, can be obtained and applied to the quantitative detection of T-DNA. As for the gDNA-G, the concentration of wild-type was quantified by the fluorescence quenching of pterin. As shown in Fig. 4B, the value of $N_{\Delta\text{Fpterin}}$ decreases gradually with the increase of $c_{\text{gDNA-G}}$. A good linear correlation to the W-DNA in the concentration range from 60 nM to 1 μM (280 – 4689 ng/mL) was obtained. The linear equation of $N_{\Delta\text{Fpterin}} = -0.364c_{\text{gDNA-G}} + 0.034$ ($R = 0.9216$) can be obtained for the quantitative detection of W-DNA. It has been reported that the concentration of T-DNA and W-DNA in peripheral blood of patients with advanced cancer are 1000 – 2000 ng/mL,[36] but 100 – 200 ng/mL[37] in healthy individuals. Therefore, the dynamic range of our method can meet the requirements for the detections of W-DNA and T-DNA in clinical peripheral blood samples.

Finally, the applicability of the tri-color fluorescence sensor was assessed in 10-fold diluted serum samples from healthy persons added with W-DNA and T-DNA. As listed in Tables 2

and 3, no KRAS gene can be detected in blank human serum samples. It is accordant with the reported low abundance in healthy individuals, which is out of the dynamic range of our method. With the addition of T-DNA and W-DNA from nM to μM, all the recoveries are above 95% and the RSD values are within 8.5%. The good performance of the tri-color fluorescence sensor strongly confirms its applicability for detection in real samples.

Conclusions

In summary, to monitor the mutation level in diverse KRAS point mutations, we developed a pterin-FAM-TAMRA tri-color sensing system to detect the T-DNA and W-DNA in one-step. In our system, the initial structure of the sensor is evaluated with the disappearance of the fluorescence response of FAM. The detection of T-DNA is based on the broken hairpin structure and the fluorescence recovery of both FAM and TAMRA. The detection of W-DNA is based on the AP site-induced guanine/pterin specific binding. Compared with the expensive and cumbersome clinical gene sequencing methods, our tri-color fluorescence sensor is time saving (the entire construction and detection period can be completed within 4 h), and is easy to assemble and operate. Meanwhile, this biosensor has an effective concentration range for detecting KRAS point mutations. This system is available for the monitoring of mutation levels in all kinds of KRAS point mutations in codon G12 (G → A, G → C, and G → T). It offers significant benefits for monitoring the clinical treatment progress and greatly improving the personalized therapy and therapeutic evaluation of patients with most types of KRAS-related cancer.

Acknowledgements

The work was financially supported by the National Natural Science Foundation of China (21573290), the Open Research Fund of State Key Laboratory of Physical Chemistry of Solid Surface, Xiamen (201814), and the State Key Laboratory of Fine Chemicals, Dalian University of Technology (KF1910).

References

1. Q. Li, D. H. Zhou, J. F. Pan, Z. Liu, and J. H. Chen, *Analyst*, **2019**, *144*, 3088.
2. O. Kranenburg, *Biochim. Biophys. Acta*, **2005**, *1756*, 81.
3. C. Almoguera, D. Shibata, K. Forrester, J. Martin, N. Arnheim, and M. Perucho, *Cell*, **1988**, *53*, 549.
4. A. K. Arrington, E. L. Heinrich, W. Lee, M. Duldulao, S. Patel, J. Sanchez, J. Garcia-Aguilar, and J. Kim, *Int. J. Mol. Sci.*, **2012**, *13*, 12153.
5. S. Forbes, J. Clements, E. Dawson, S. Bamford, and M. R. Stratton, *British Journal of Cancer*, **2006**, *94*, 318.
6. D. J. Hartman, J. Davison, T. Foxwell, M. N. Nikiforova, and S. I. Chiosea, *Int. J. Cancer*, **2012**, *131*, 1810.
7. A. Lièvre, J.-B. Bachet, V. Boige, A. Cayre, D. L. Corre, E. Buc, M. Ychou, O. Bouché, B. Landi, C. Louvet, T. André, F. Bibeau, M.-D. Diebold, P. Rougier, M. Ducreux, G. Tomasic, J.-F. Emile, F. Penault-Llorca, and P. Laurent-Puig, *J. Clin. Oncol.*, **2008**, *26*, 374.
8. F. Sanger, *Science*, **1981**, *214*, 1205.
9. S. Ogino, T. Kawasaki, M. Brahmandam, L. Yan, M. Cantor, C. Namgyal, M. Mino-Kenudson, G. Y. Lauwers, M. Loda, and C. S. Fuchs, *J. Mol. Diagn.*, **2005**, *7*, 413.
10. D. Simant, Q. Jian, R. Ramesh, and W. Xiaolin, *Plos One*, **2008**, *3*, e2876.
11. R. K. Patel, J. Mukesh, and L. Zhanjiang, *Plos One*, **2012**, *7*, e30619.
12. S. Hussung, M. Follo, R. F. U. Klar, S. Michalczyk, K. Fritsch, F. Nollmann, J. Hipp, J. Duyster, F. Scherer, N. von Bubnoff, M. Boerries, U. Wittel, and R. M. Fritsch, *J. Mol. Diagn.*, **2020**, *22*, 943.
13. Y. F. Huang, M. L. Tao, S. H. Luo, Y. Zhang, B. Situ, X. Y. Ye, P. W. Chen, X. J. Jiang, Q. Wang, and L. Zheng, *Anal. Chim. Acta*, **2020**, *1107*, 40.
14. Y. S. Wang, S. L. Kong, and X. D. Su, *RSC Adv.*, **2020**, *10*, 1476.
15. J. D. Luo, E. C. Chan, S. Chun-Liang, T. L. Chen, L. Ying, H. Tsann-Long, and C. Chiuan-Chian, *Nucleic Acids Res.*, **2006**, *34*, e12.
16. C. Fernández-Vega, D. C. García-Olmo, M. A. Ballesteros, and D. García-Olmo, *Mol. Biotechnol.*, **2002**, *22*, 115.
17. S. Yamada, M. Yashiro, K. Maeda, Y. Nishiguchi, and K. Hirakawa, *Int. J. Cancer*, **2005**, *113*, 1015.
18. S. L. Lilleberg, J. Durocher, C. Sanders, K. Walters, and K. Culver, *Ann. N. Y. Acad. Sci.*, **2004**, *1022*, 250.
19. N. Zeng and J. Xiang, *Talanta*, **2019**, *198*, 111.
20. J. L. Bos, E. R. Fearon, S. R. Hamilton, M. V. d. Vries, J. H. van Boom, A. J. van der Eb, and B. Vogelstein, *Nature*, **1987**, *327*, 293.
21. K. Forrester, C. Almoguera, K. Han, W. E. Grizzle, and M. Perucho, *Nat. Med.*, **1987**, *327*, 298.
22. G. C. Burmer and L. A. Loeb, *Proc. Natl. Acad. Sci. U. S. A.*, **1989**, *86*, 2403.
23. G. Capella, S. Cronauer-Mitra, M. A. Pienado, and M. Perucho, *Environ. Health Perspect.*, **1991**, *93*, 125.
24. S. D. Finkelstein, R. Sayegh, S. Christensen, and P. A. Swalsky, *Cancer*, **1993**, *71*, 3827.
25. J. J. Oudejans, R. J. C. Slebos, F. A. N. Zoetmulder, W. J. Mooi, and S. Rodenhuis, *Int. J. Cancer*, **1991**, *49*, 875.
26. J. Neumann, E. Zeindl-Eberhart, T. Kirchner, and A. Jung, *Pathol. Res. Prac.*, **2009**, *205*, 858.
27. V. Taly, D. Pekin, L. Benhaim, S. K. Kotsopoulos, D. Le Corre, X. Li, I. Atochin, D. R. Link, A. D. Griffiths, and K. Pallier, *Clin. Chem.*, **2013**, *59*, 1722.
28. M. Zhang, J. Chen, X. Pi, C. Deng, and J. Xiang, *Electroanalysis*, **2019**, *31*, 477.
29. H. M. Fang, N. L. Xie, M. Ou, J. Huang, W. S. Li, Q. Wang, J. B. Liu, X. H. Yang, and K. M. Wang, *Anal. Chem.*, **2018**, *90*, 7164.
30. C. I. Richards, J.-C. Hsiang, A. M. Khalil, N. P. Hull, and R. M. Dickson, *J. Am. Chem. Soc.*, **2010**, *132*, 6318.
31. Q. Wang, M. Pan, J. Wei, X. Liu, and F. Wang, *ACS Sens.*, **2017**, *2*, 932.
32. S. Xu, Y. Shao, K. Ma, Q. Cui, G. Liu, and F. Wu, *Sens Actuators, B*, **2012**, *171–172*, 666.
33. K. Yoshimoto, C. Y. Xu, S. Nishizawa, T. Haga, and N. Teramae, *Chem. Commun.*, **2004**, *9*, 2960.
34. H. Mao, G. Luo, Y. Zhan, J. Zhang, S. Yao, and Y. Yu, *Analyst*, **2018**, *143*, 3292.
35. M. W. Karaman, S. Groshen, C.-C. Lee, B. L. Pike, and J. G. Hacia, *Nucleic Acids Res.*, **2005**, *33*, e33.
36. A. R. Thierry, F. Mouliere, S. El Messaoudi, C. Mollevi, E. Lopez-Crapez, F. Rolet, B. Gillet, C. Gongora, P. Dechelotte, B. Robert, M. Del Rio, P.-J. Lamy, F. Bibeau, M. Nouaille, V. Loriot, A.-S. Jarrousse, F. Molina, M. Mathonnet, D. Pezet, and M. Ychou, *Nat. Med.*, **2014**, *20*, 430.
37. E. Gormally, P. Hainaut, E. Caboux, L. Airoldi, and P. Vineis, *Int. J. Cancer*, **2004**, *111*, 746.